Available online at www.sciencedirect.com

ScienceDirect

MATTER AND RADIATION AT EXTREMES

Matter and Radiation at Extremes 2 (2017) 278–286

www.journals.elsevier.com/matter-and-radiation-at-extremes

Review Article

The pulsed high magnetic field facility and scientific research at Wuhan National High Magnetic Field Center

Xiaotao Han, Tao Peng, Hongfa Ding, Tonghai Ding, Zengwei Zhu, Zhengcai Xia, Junfeng Wang, Junbo Han, Zhongwen Ouyang, Zhenxing Wang, Yibo Han, Houxiu Xiao, Quanliang Cao, Yiliang Lv, Yuan Pan, Liang Li*

Wuhan National High Magnetic Field Center, Huazhong University of Science and Technology, Wuhan, 430074, China

Received 21 July 2017; revised 16 October 2017; accepted 19 October 2017
Available online 13 November 2017

Abstract

Wuhan National High Magnetic Field Center (WHMFC) at Huazhong University of Science and Technology is one of the top-class research centers in the world, which can offer pulsed fields up to 90.6 T with different field waveforms for scientific research and has passed the final evaluation of the Chinese government in 2014. This paper will give a brief introduction of the facility and the development status of pulsed magnetic fields research at WHMFC. In addition, it will describe the application development of pulsed magnetic fields in both scientific and industrial research.

PACS codes: 07.55.Db; 07.55.-w; 01.50.Pa

Keywords: Pulsed high magnetic field; Pulsed magnet; Scientific research; Electromagnetic technology

1. Introduction

High magnetic field is an important tool for scientific research and industrial applications, such as solid state physics, chemistry, medicine and high-energy physics [1]. Typically, there are two kinds of non-destructive high magnetic field: continuous magnetic field and pulsed magnetic field. Compared with the former, the latter has much higher field strength, and it will play a more important and practical role in researches related with high field strength. Up to now, the 100-T non-destructive magnet at the National High Magnetic Field Laboratory (NHMFL) can overcome the mega-gauss barrier to produce 100.75 T field (world record) [2]. The peak field of 94.2 T was produced in the Dresden High Magnetic Field Laboratory in Germany [3]. The Laboratoire National des Champs Magnétiques Intenses (LNCMI) has also developed a user magnet at the level of 90 T [4].

The pulsed high magnetic field facility at Wuhan National High Magnetic Field Center (WHMFC) was funded by the Chinese National Development and Reformation Committee (NDRC) [5]. After 5 years of intensive work, the construction of the facility has accomplished all the goals of the research proposal and the developed high field facility could provide many opportunities for scientists in research fields including solid state physics, chemistry, medicine, plasma science and high-energy physics. This paper will present the performance of the high magnetic field facility and research work relevant to magnetic fields at WHMFC.

* Corresponding author.
E-mail address: liangli44@mail.hust.edu.cn (L. Li).

Peer review under responsibility of Science and Technology Information Center, China Academy of Engineering Physics.

https://doi.org/10.1016/j.mre.2017.10.002

2. Pulsed high magnetic field facility at WHMFC

As a national research institute, WHMFC is one of the accomplishments of National Major Science and Technology Infrastructure Projects in China's Eleventh Five-Year Plan. In 2014, the construction of the pulsed high magnetic field facility was completed at WHMFC and available for public users. The facility is composed of three types of power supply, several pulsed magnets, a control system, four types of experimental stations and a cryogenic system.

2.1. Power supply

Three types of pulsed power supply, including a 25.6 MJ/25 kV capacitor bank, a 100 MVA flywheel (pulse) generator and a new type of lead-acid battery bank, have been developed. The capacitor bank consists of 24 independent 1 MJ modules with a short circuit current of 45 kA each and 2 independent 0.8 MJ modules of 60 kA each. The 26 modules can be flexibly employed to meet the requirements of different magnets for 50–90 T magnetic fields with different pulse durations. The battery bank power supply consists of 900 batteries (model: 12 V/200 Ah/2000 A in 2 s), and a 35 kA thyristor DC switch has been developed.

2.2. Pulsed magnet

Typical pulsed magnets at WHMFC are the capacitor bank driven monolithic coils. They are all made of soft copper or CuNb wires, internally and externally reinforced by Zylon, glass or carbon fiber. Note that Zylon, a poly-p-phenylenebenzobisoxazole (PBO), is a high-performance fiber developed by Toyobo Corporation. The world's highest peak field of pulsed magnet made of soft copper is 75 T in a 12 mm bore at WHMFC. In order to reduce the cooling time after a high field pulse, we introduced cooling channels in the middle of the winding. For a 60 T pulse in a 21 mm bore, this technology decreased the cooling time from 160 min down to 35 min [6]. This kind of magnet is now routinely used for experiments at WHMFC. A dual stage magnet with 12 mm bore had been designed and it successfully obtained 86.3 T non-destructively in the experiments. Inspired by the test results, a duplicate magnet was developed and a peak field of 90.6 T was obtained.

2.3. Control system

The user-friendly control and measurement system has two parts: the local control-measurement system at the measurement cells and the central control system in the control room. These two systems are connected via optical fiber transmission for galvanic isolation. A PLC (Programmable Logical Controller) system is applied to control the switches, relays and thyristors of the capacitor bank. The key signals of source voltage, coil current and magnetic field in the coil center are measured by a 24 bits, 200 kHz sample rate DAQ (Data Acquisition) card, in which the field strength is calibrated by the de Haas-van Alphen effect of polycrystalline copper.

2.4. Experimental station

Experimental stations including electric transport, magnetization, magneto-optics and electron spin resonance (ESR) can be used in parallel. Equipments such as low temperature cryostats (from 50 mK to 400 K), high pressure cells and various lasers with associated optical systems have been installed.

2.5. Cryogenic system

The cryogenic system includes cryostats for scientific experiments, a helium recovery system, a system for the supply of liquid nitrogen and other gases. The main cooling methods for scientific experiments include helium-4 cryostats, helium-3 cryostats, gas-flow cryostats and a dilution refrigerator. In addition to these types of cryostats, a cryogen-free cryostat based on a small GM cryocooler has been developed. The helium-3 and helium-4 cryogenic systems cover the temperature range from 400 mK to 300 K, and the dilution refrigerator system has reached 39 mK.

3. Pulsed magnetic field research at WHMFC

Several types of pulsed magnetic field systems have been developed at WHMFC as listed in Table 1 [7]. Three typical fields are introduced in detail in the following subsections.

3.1. High-strength magnetic field

At WHMFC, a dual-stage coil system has been developed that so far generated 90.6 T maximum field non-destructively [8]. The experimental results are shown in Fig. 1. The magnet bore diameter is 12 mm. The inner coil is energized by the 1.6 MJ/25 kV module (combination of two 0.8 MJ modules) and the outer coil by eleven 1 MJ/25 kV modules. The inner coil consists of 8 layers of 2.8 mm × 4.3 mm CuNb microcomposite wire developed by China Northwest Institute for Non-ferrous Metal Research of China. The outer coil is made of 12 layers of 4 mm × 8 mm soft copper that is wound directly on the inner coil.

Table 1
Developed high magnetic field facilities.

Magnet type	Power supply	Field strength	Bore diameter	Pulse duration	Remarks
Monolithic coil	Capacitor bank	50–75 T	12–34 mm	20–200 ms	User magnet
Dual-coil	Capacitor bank	75–90.6 T	12–14 mm	~100 ms	Max. 90.6 T
Dual-coil	Pulsed generator	50 T	22 mm	1 s	100 ms flat-top, 0.4% ripple
Monolithic coil	Battery bank	34 T	22 mm	1 s	Stability ~100 ppm

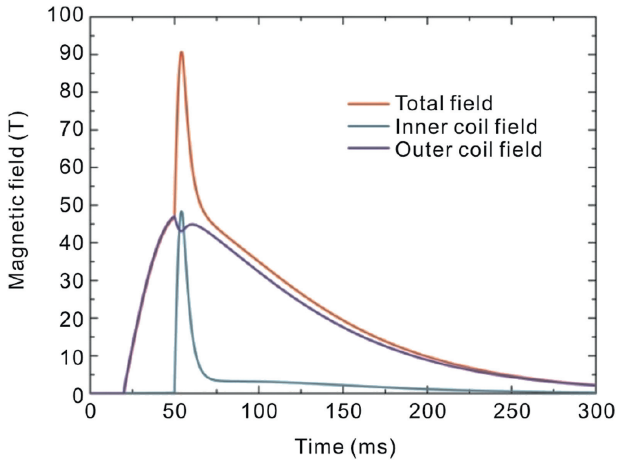

Fig. 1. Measured field waveforms of the 90.6 T field.

Magnetic field design targeting at 100 T has been proposed [9] and the 100 T project is ongoing. The designed magnet consists of three coils and will be energized by the combination of three types of pulsed power supply including a capacitor bank system, a pulse generator system and a lead-acid battery bank system.

3.2. Long-pulse magnetic field

To obtain magnetic fields with long pulse width, two types of power systems have been developed at WHMFC, including a flywheel generator and a battery power system. As shown in Fig. 2, a 50 T/100 ms flat-top field in a 22 mm bore was generated [10], in which the magnetic field ripples of 100 ms flat-top are less than 0.5%. The 50 T long pulse magnet powered by the pulsed generator consists of two coaxially nested coils. The coils are 250 mm in height. Each self-supporting coil is designed based on the fabrication principle of monolithic magnets. The two coils are each powered by one rectifier unit. The inner coil consists of 12 layers of 4 mm × 6 mm soft copper wire and each layer is reinforced by the Zylon. The inner coil provides 30 T at 14 kA peak current. The outer coil consists of 18 layers of 5 mm × 10 mm soft copper. The outer coil will provide a 20 T, 2000 ms background field at 15 kA current.

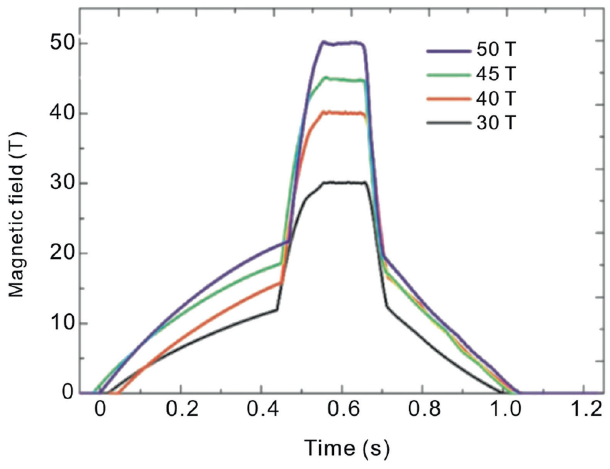

Fig. 2. 50 T long pulsed magnetic field.

As shown in Fig. 3, a peak field of 35.8 T/2 s in 22 mm bore was achieved using a magnet consisting of a poly-helix inner coil and a copper foil outer coil [11], in which the two coils are connected in series. The poly-helix coil has 9 layers and each layer is reinforced by Zylon-epoxy composite. The outer coil is wound with copper foil to provide low inductance and resistance for the magnet. It is externally reinforced by the carbon fiber.

3.3. High-stability (pulse flat-top) magnetic field

Besides the field strength, the pulse fields with flat-top (high stability) are desired for scientific research. The magnetic field waveform with flat-top in Fig. 4 was obtained using the PWM (Pulse Width Modulation) controlled bypass circuit. So far, the fields range from 10 T to 25 T with stability of 100–200 ppm and flat-top of 200–400 ms [12]. The development of this facility is still in progress. This project is aimed at field more than 40 T and flat-top time more than 200ms.

Apart from the above mentioned methods, a new method for obtaining a flat-top pulsed magnetic field using two capacitor banks was proposed at WHMFC [13]. Experiments were carried out to generate flat-top fields of about 10 T, 20 T and 40 T, and the field curves have 10 ms flat-top at the stability of 1%, as shown in Fig. 5. More data of test sequences can be found in our previous work [13]. The technology can be transferred to all the other pulsed magnets which are now in operation. It is quite possible to produce fields in the range of 60–80 T with flat-top.

4. Scientific research at WHMFC

4.1. Electrical transport station

The electrical transport stations are able to measure conducting materials by magneto-resistance and/or Hall effect under extreme conditions: temperature from room-temperature down to 1.6 K and magnetic fields up to 65 T with regular magnets. More extreme conditions are available: the temperature could be lowered to 0.4 K using ^{3}He and the magnetic field could reach 90.6 T if requested by users for their specific experiments. We carry out transport measurements either with direct current (DC) or alternating current (AC) methods depending on samples. If the resistance of a sample is 100 mΩ–1000 Ω, AC method is implemented with a typical current of 5 mA at around 100 kHz; and DC is applied once the resistance of a sample excesses 1000 Ω. Though we can achieve high accuracy by phase-locking with the AC method, the contact resistance is the main issue since it will induce a capacitance between sample and signal wires, which is harmful to increasing the signal frequency. The relative accuracy can reach 0.05 mΩ in the optimal configuration by reducing the contact resistance on sample and mechanical vibration of the probe simultaneously. A sample dimension of 2 mm × 1 mm × 0.5 mm is preferred for minimizing the eddy current.

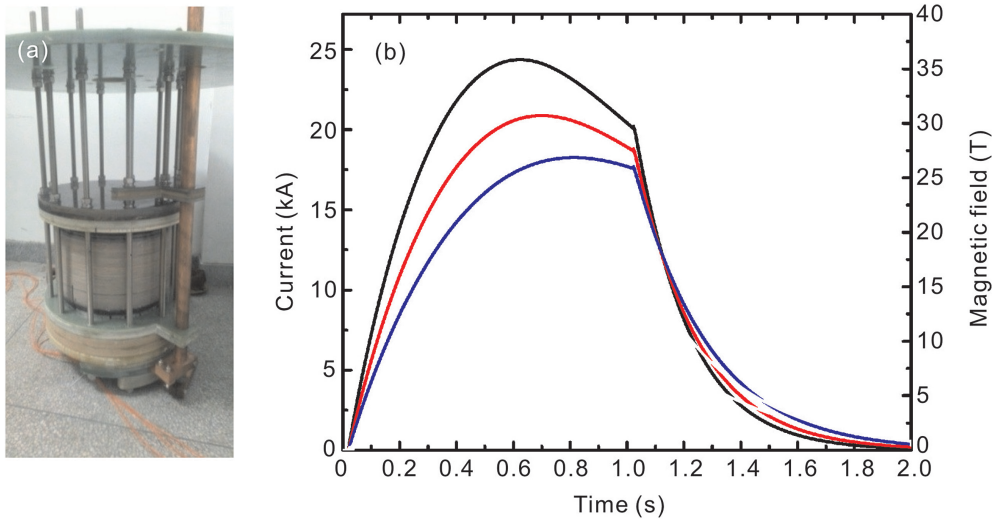

Fig. 3. Photo of (a) the magnet and (b) the magnetic field waveform.

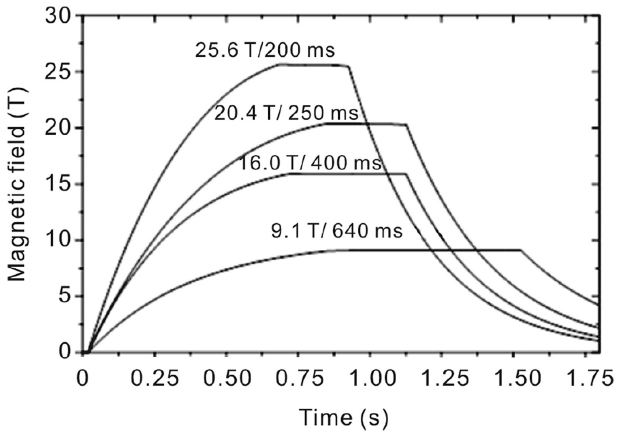

Fig. 4. 25 T/200 ms flat-top with high stability.

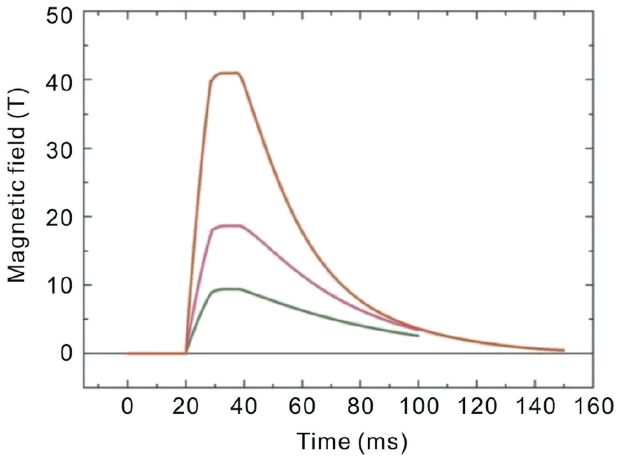

Fig. 5. Measured field waveform with flat-top.

The main researches performed by staff and users in electrical transport stations have been focusing on properties of superconductors and topological materials. For instance, some intriguing properties of topological materials have been revealed by our facility. In Dirac semimetal Cd_3As_2, Faxian Xiu extended their magneto-resistance measurement up to 52 T, revealing high magnetic field can tune the Dirac semimetal into a Weyl semimetal phase [14]. We refer readers to references [15–17] for more interesting work on topological materials. Superconductors, especially with high upper-critical field (H_{c2}), are the majority of the materials studied at our facility. Their H_{c2} which closely links to superconductivity can only be extracted under high fields. Iron-based superconductors are frequently studied at our facility for their high H_{c2} [18]. How the 3D electrons behave far beyond their quantum limit is another intriguing topic being studied in our center. Fig. 6 shows an example based on an extensive set of angle-dependent magnetoresistance data, and it is revealed that one or two electron valleys of bismuth can be totally emptied by ultra-strong magnetic fields [19]. Notice that, certain topological materials are also dilute metals. Exotic phenomena would be also induced by ultrahigh fields, for instance [20].

4.2. Magnetization station

The magnetization station is one of the most important measurement systems for pulsed high field facilities in the world. This experimental technique is very popular because many magnetic materials are of particular interests due to the field-induced magnetic phase transitions. The transitions often occur when the external magnetic field can compete with the exchange interactions, magnetic anisotropy, Dzyaloshinsky-moriya interaction, electron correlation, etc. in these materials. A sufficient high magnetic field can change the spin or magnetic structure of the materials and therefore cause a dramatic change of magnetic moment in magnetization.

The magnetization in a pulsed field was measured by an induction method using a well-compensated pick-up coil. The dM/dt signal from the sample was collected and integrated after comparison of the results of two different pulse shots—sample-in and sample-out. Apart from the high

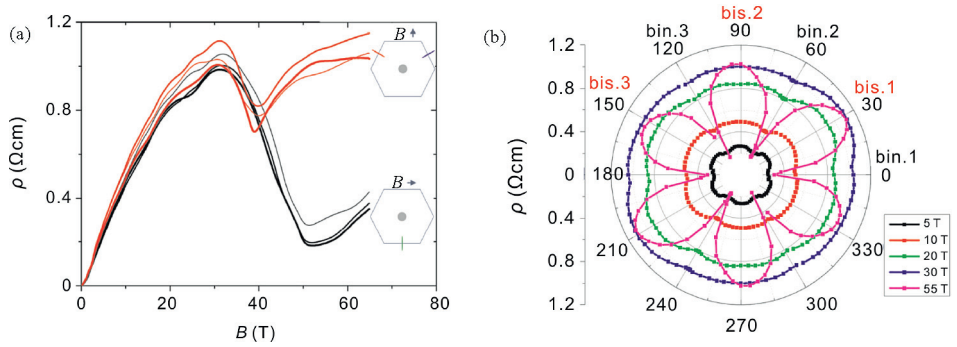

Fig. 6. (a) Magnetoresistance of a bismuth crystal up to 65 T at 1.65 K for magnetic fields along three binary (in black) and bisectrix axes (in red). (b) Polar plot of angle dependence of magnetoresistance for different fields. Note the dramatic enhancement of angular magnetoresistance oscillations at 55 T, relating to the emptying electron valleys [19].

strength of the magnetic fields, this technique takes two other distinct advantages in comparison with the measurement in a steady field. It is very sensitive to detect weak magnetic phase transitions due to its very short measuring time (6–60 ms) and the high-speed (>250 k/s sampling rate) data acquisition system. Further, the field-sweeping rate is very high and some spin dynamic issues can be studied by tuning the field-sweeping rate to 10^3–10^5 T/s.

In WHMFC, two magnetization stations are installed with a short-pulse (6–12 ms) magnet and a long-pulse (40–60 ms) magnet for insulating and metallic samples, respectively, due to the eddy current effect on the metallic samples. The peak-fields of the pulsed fields range from 50 T to 75 T. Measuring temperatures vary from 400 K to 1.5 K with the helium-4 system and it is further lowered down to 0.4 K using a helium-3 system. Our facility also offers opportunity to study the magnetic properties such as magnetostriction, electric polarization, magnetic torque, etc. associated with the field-induced magnetization transitions in magnetic materials. These unique experimental techniques play an essential role to reveal the underlying magnetism and to explore novel quantum states in magnetic materials, for instance, perovskite manganites, multiferroics, Bose-Einstein condensation system, heavy fermions, etc. Series of high-field magnetization measurements have been performed in the following research fields: frustrated magnets, spin chains and Bose-Einstein condensates [21–24]. Fig. 7 shows the high field magnetization studies of multiferroic $CuFeO_2$ single crystal grown by an optical floating zone method [22]. We observed a series of field-induced multi-step-like transitions, in which the critical magnetic fields were temperature-dependent and magnetic anisotropic. With a systematical measurement, a complete magnetic and multiferroic H-T phase diagram is depicted in fields up to 75 T [22].

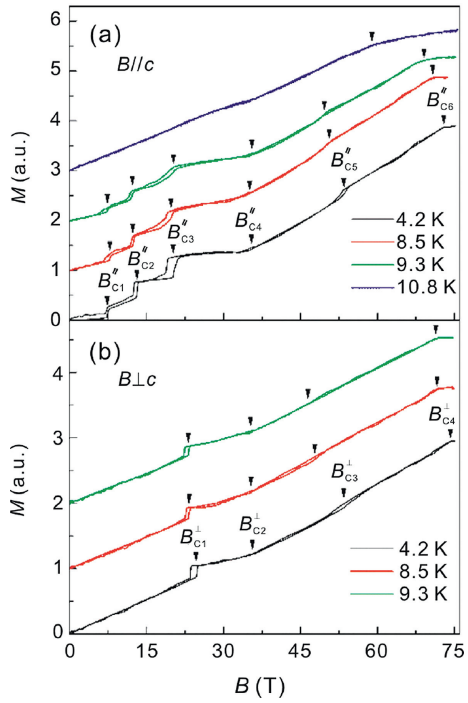

Fig. 7. Magnetic field dependence of the magnetization behavior of $CuFeO_2$ with the applied field (a) parallel to the c axis and (b) perpendicular to the c axis measured at various temperatures [22].

4.3. Magneto-optics station

The magneto-optics station has been constructed to realize the optical spectra measurements including the absorption, reflection, photoluminescence, magneto-Kerr and Faraday rotation in pulsed high magnetic fields. The light sources and optical detectors cover the wavelength range from near-ultraviolet to near-infrared (300–1600 nm). In this region, various materials including semiconductors [25], rare-earth fluorescent material [26–28], and ferro- and antiferro-magnets could be investigated. The magnetic and optical parameters, such as the optical band gap, the electronic effective mass and the local crystal field symmetry of the luminescence centers could be revealed, which are essentially important for their applications in photovoltaic system, optical display, LED, and magnetic storage.

The high magnetic field photoluminescence is extremely suitable for the investigation of rare-earth luminescent crystals. For example, when luminescence ions are doped in different dielectric crystal lattices, their dopant sites

environment, which is often concealed by the crystal field splitting at zero and low magnetic fields, could be easily revealed from the high field Zeeman splitting. Fig. 8 shows the clearly distinct high field Zeeman splitting patterns of Eu^{3+} dopant in different local sites [27]. It is shown that, not only the site symmetry, but also the local magnetic environments could be distinguished. The exploration of the site symmetry is important for the manipulation of optical emission bands and the design of many optical devices.

4.4. Electron spin resonance station

Electron spin resonance (ESR) is a powerful spectroscopic technique to study the magnetic materials from condensed matter physics to biology and chemistry. High field ESR is particularly favored because of its advantages over low field ESR as follows: 1) higher absolute sensitivity; 2) some high-spin systems cannot be accessed at low frequencies; 3) higher Zeeman resolution (and orientation selection); 4) high-field phases; 5) higher electron spin polarization; 6) faster timescale, etc. Based on the pulsed magnets developed at WHMFC, the first high field ESR system in China was established in 2012 [29]. The facility can achieve a frequency range of 60–550 GHz, magnetic fields up to 50 T and a temperature range of 2–300 K.

Using the ESR facility in WHMFC, various kinds of magnetic materials have been studied, including organic radicals, single molecule magnets, quantum spin systems, and others. For example, high-field ESR measurements of an antiferro-magnet Ca_3ZnMnO_6, isostructure with the Ising-chain multiferroic Ca_3ZnMnO_6, have been carried out. The zero-field spin gap is derived to be about 166 GHz, originating from the easy-plane anisotropy and exchange interaction. Our results suggest that the Dzyaloshinsky–Moriya interaction is absent (Fig. 9(a) and (a′)) [30]. The axial zero field splitting parameter was unambiguously determined by the high field ESR technique and magnetic measurements. The obtained result shows the first observed single-molecule-magnet behavior in the square planar coordination geometry of any metal ions (Fig. 9(b) and (b′)) [31].

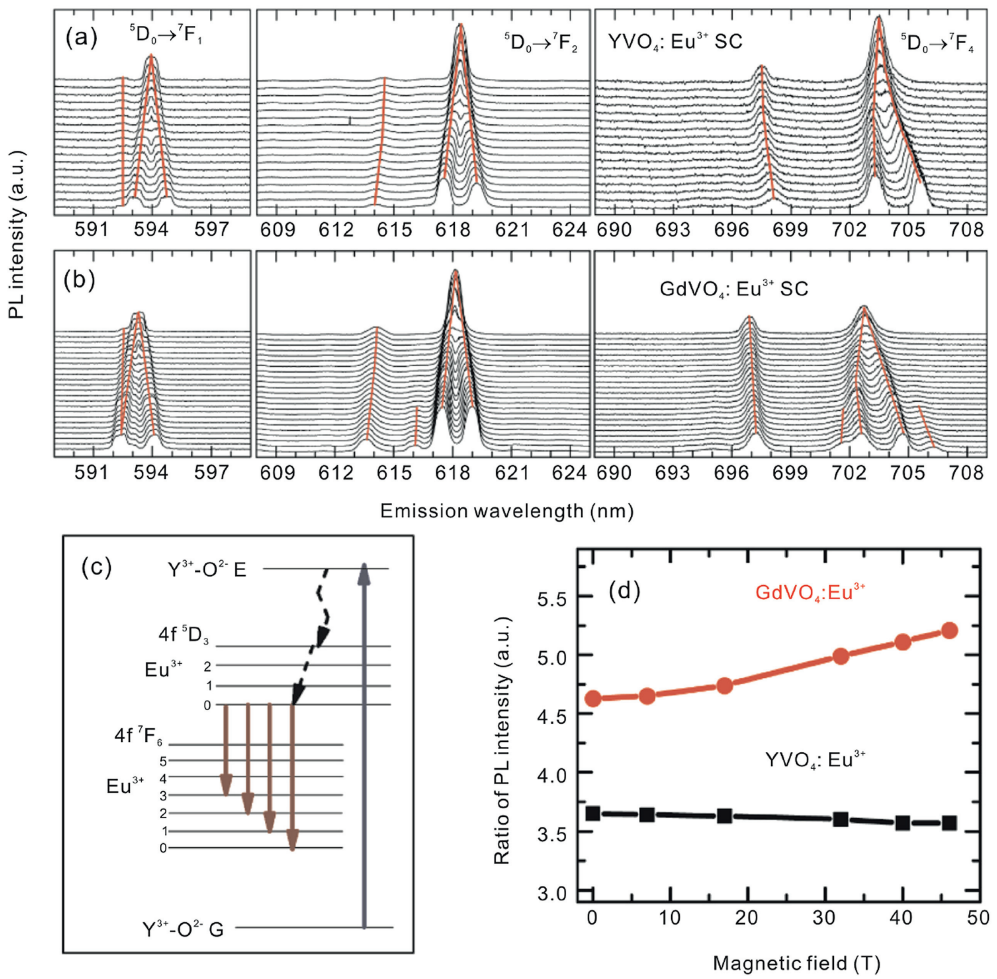

Fig. 8. Magneto-photoluminescence spectra of Eu^{3+} doped in (a) YVO_4 and (b) $GdVO_4$ [27] for magnetic field from 0 T (upper) to 46 T (down). The solid lines crossing the curves indicate the trace of the peaks. The energy diagram of the YVO_4:Eu^{3+} is shown in (c), and the ratio of PL intensity of the electric dipole transition to that of the magnetic dipole transition is shown in (d).

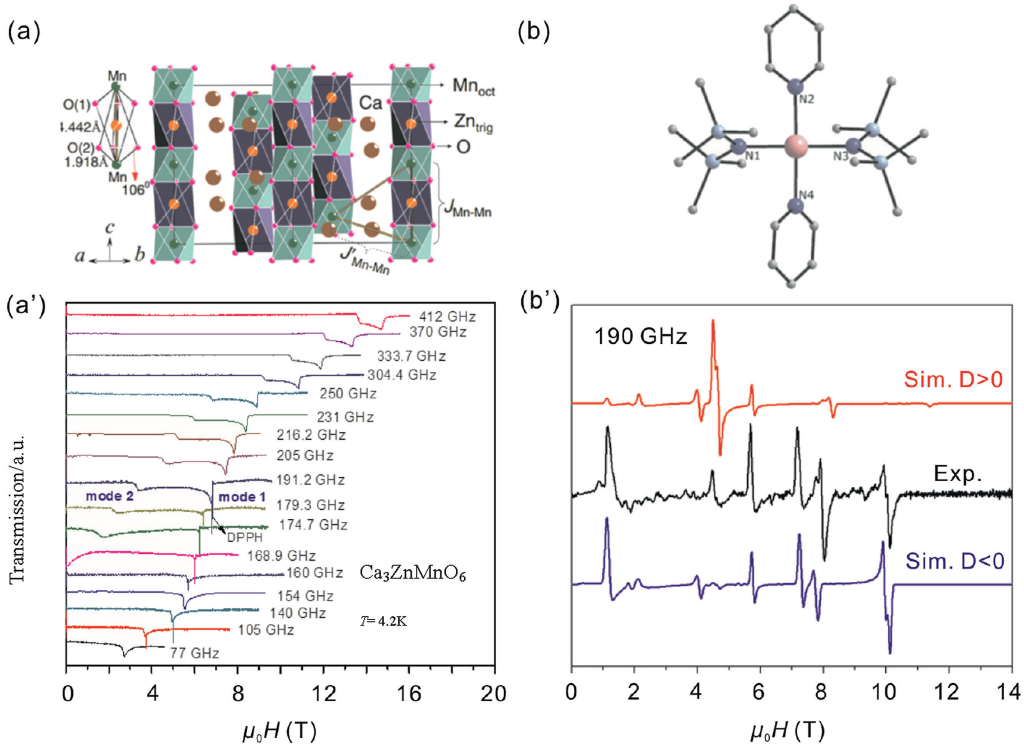

Fig. 9. (a, a′) The crystal structure of Ca_3ZnMnO_6 and its high field ESR spectra, respectively. (b, b′) The crystal structure of Cr-Py and its high field ESR spectra, respectively.

5. Electromagnetic applications at WHMFC

5.1. Electromagnetic forming

High-performance light-weight sheet and tube parts as well as their manufacturing technology occupy a pivotal position in the field of advanced manufacturing, which is an important safeguard of achieving light-weight equipment for enhanced performance, energy conservation and environmental protection. Light-weight materials, represented by aluminum alloys, have a poor forming performance using the traditional quasi-static stamping process, such as easy fracture, large spring-back and poor surface quality. Electromagnetic forming with features of high-speed, non-contact and single-die is considered to be one of the most promising methods to solve these problems [32]. However, the pulsed electromagnetic forces are not strong enough and hard to be adjusted in the existing electromagnetic field (EMF) systems due to single-coil and single-power model, which has restricted its extensive applications in forming large-scale and complex sheets [33].

To solve the current bottleneck problems of the EMF technology, a Space-Time-Controlled Multi-Stage Pulsed Magnetic Field (Stic-Must-PMF) forming and manufacturing technology has been proposed in our previous work [33]. Strong electromagnetic forces can be generated by introducing the nondestructive pulsed high field magnet technology to fabricate tool coils with high strength and long life performance. Meanwhile, the distribution of these forces acting on the workpiece can be well adjusted by using multiple tool coils and several sets of pulsed power systems, in which each coil is energized individually by different power supplies with a precise timing control. To validate the effectiveness of this improved EMF technology, a three-stage forming system with three types of pulsed power supply and a timing control system had been developed at WHMFC, and several studies were carried out for large-scale sheet forming [34,35], deep drawing of sheet metal [36] as well as tube forming [37].

5.2. Post-assembly magnetization

Permanent magnet (PM) motors are widely used thanks to their outstanding advantages of high efficiency and energy saving. The permanent magnets are usually pre-magnetized and then assembled on the motors. The pre-magnetized magnets should be handled with great care during the assembly process to prevent them from damage or potential dangers for workers because of the very strong attractive or repulsive magnetic force. One effective solution to this problem is to magnetize the permanent magnets after the rotor is assembled or the motor is completely assembled [38]. Post-assembly magnetization not only simplifies the assembly process, reduces the cost, but also improves the performance of the motor.

One common method for post-assembly magnetization is to magnetize the permanent magnets by a pulse of high current through the stator winding after complete assembly. But this method mainly aimed at small motors due to the fact that the magnetizing current is prohibited by the stator windings. We

focus on magnetizing the motor by a specially designed magnetizing device or by integrated magnetizing windings. For the rotor of a 100 kW high speed PM motor, a magnetizing fixture consisting of three magnetizing coils was specially designed [39]. The rotor has a total length of 515 mm and an outer diameter of 80 mm, in which the pole length is 285 mm. It is designed as a two-pole rotor with parallel magnetization. The magnetizing fixture energized by two 1MJ capacitor bank modules can produce a peak field of 6 T to fully magnetize the assembled rotor. For the surface mounted and insert type PM motors, the magnetizing windings are directly wound on the outer surface of the permanent magnet, and then assembled on the motor. The PM poles can be magnetized and demagnetized after assembly by the integrated magnetizing windings. Once the PM poles experience demagnetization fault, the magnetizing windings can magnetize the PM poles again without disassemble of the motor. The integrated magnetizing windings of a 2 MW PM wind generator and a 20 kW PM synchronous motor were designed. The magnetizing test revealed that the PM poles could be successfully magnetized and demagnetized by the magnetizing winding.

5.3. Magnetic manipulation

Manipulation of particle motion by magnetic fields is an effective technique for localization and transport of micro-and nano-materials [40]. Due to several advantages including multifunctionality, targetablity, controllability and noncontact, the technique has attracted growing interest in various biological and chemical applications such as drug targeting for medical treatment [41], gene delivery [42] and particle separation [43].

Based on this technique, several numerical and experimental studies have been carried out at WHMFC, including magnetic drug delivery [44], magnetic separation [45] and mixing [46] in microfluidics. For example, we have adapted the principle of magnetic manipulation in the activation process of G protein-coupled receptor (GPCR) [44]. In the conventional activation process, the activation efficiency of GPCR is relatively low due to insufficient contact of drug with target cells. To solve this problem, a gradient magnetic field generated by an electromagnetic system has been applied to produce magnetic force for delivering the drugs carrying magnetic nanoparticles to the bottom of the plate. Then the drug concentration around the cell-surface receptors can be greatly improved. Experimental results show that the activation efficiency of GPCR can be increased about 6 times with the aid of the principle of magnetic manipulation.

6. Conclusion

This paper summarizes the development of the pulsed high magnetic field facility at WHMFC including power supplies, magnets, control system and experimental stations. The facility will provide an outstanding research platform and many research opportunities for the scientific communities in China and abroad. Meanwhile, the in-house staff of WHMFC has carried out some research projects on the applications of pulsed power and high field techniques, such as electromagnetic forming and post-assembly magnetization of permanent magnet rotor. WHFMC has the ability to provide high pulsed magnetic fields for scientific research and technological applications.

Acknowledgments

We gratefully acknowledge the financial support of the National Key Research and Development Program of China (2016YFA0401700).

References

[1] F. Herlach, High Magnetic Fields: Science and Technology, World Scientific, 2003.
[2] D.N. Nguyen, J. Michel, C.H. Mielke, Status and development of pulsed magnets at the NHMFL pulsed field facility, IEEE Trans. Appl. Supercond. 26 (4) (2016) 4300905.
[3] S. Zherlitsyn, B. Wustmann, T. Herrmannsdörfer, J. Wosnitza, Magnet-technology development at the Dresden High Magnetic Field Laboratory, J. Low Temp. Phys. 170 (5) (2013) 447−451.
[4] M.D. Watson, T. Yamashita, S. Kasahara, W. Knafo, M. Nardone, et al., Dichotomy between the hole and electron behavior in multiband superconductor FeSe probed by ultrahigh magnetic fields, Phys. Rev. Lett. 115 (2) (2015) 027006.
[5] L. Li, T. Peng, H.F. Ding, X.T. Han, Z.C. Xia, et al., Progress in the development of the Wuhan high magnetic field center, J. Low Temp. Phys. 159 (1−2) (2010) 374−380.
[6] T. Peng, Q. Sun, J. Zhao, F. Jiang, L. Li, et al., Development of fast cooling pulsed magnets at the Wuhan National High Magnetic Field Center, Rev. Sci. Instrum. 84 (12) (2013) 125112.
[7] L. Li, Y.L. Lv, H.F. Ding, T.H. Ding, X.T. Han, et al., Short and long pulse high magnetic field facility at the Wuhan National High Magnetic Field Center, IEEE Trans. Appl. Supercond. 24 (3) (2014) 9500404.
[8] T. Peng, F. Jiang, Q.Q. Sun, Q. Xu, H.X. Xiao, et al., Design and test of a 90-T nondestructive magnet at the Wuhan National High Magnetic Field Center, IEEE Trans. Appl. Supercond. 24 (3) (2014) 4300604.
[9] T. Peng, F. Jiang, Q.Q. Sun, Y. Pan, F. Herlach, et al., Concept design of 100-T pulsed magnet at the Wuhan National High Magnetic Field Center, IEEE Trans. Appl. Supercond. 26 (4) (2016) 4300504.
[10] H. Ding, J. Hu, W. Liu, Y. Xu, C. Jiang, et al., Design of a 135 MW power supply for a 50 T pulsed magnet, IEEE Trans. Appl. Supercond. 22 (3) (2012) 5400504.
[11] Y.L. Lv, T. Peng, G.B. Wang, T.H. Ding, X.T. Han, et al., Magnet design and analysis of a 40 Tesla long pulse system energized by a battery bank, J. Low Temp. Phys. 170 (5−6) (2013) 475−480.
[12] H. Xiao, Y. Ma, Y. Lv, T. Ding, S. Zhang, et al., Development of a high-stability flat-top pulsed magnetic field facility, IEEE Trans. Power Electron. 29 (9) (2014) 4532−4537.
[13] F. Jiang, T. Peng, H. Xiao, J. Zhao, Y. Pan, et al., Design and test of a flat-top magnetic field system driven by capacitor banks, Rev. Sci. Instrum. 85 (4) (2014) 045106.
[14] J. Cao, S. Liang, C. Zhang, Y. Liu, J. Huang, et al., Landau level splitting in Cd_3As_2 under high magnetic fields, Nat. Commun. 6 (2015) 7779.
[15] Y. Liu, X. Yuan, C. Zhang, Z. Jin, A. Narayan, et al., Zeeman splitting and dynamical mass generation in Dirac semimetal $ZrTe_5$, Nat. Commun. 7 (2016) 12516.
[16] Y. Zhao, H. Liu, C. Zhang, H. Wang, J. Wang, et al., Anisotropic Fermi surface and quantum limit transport in high mobility three-dimensional Dirac semimetal Cd_3A_{s2}, Phys. Rev. X 5 (3) (2015) 031037.
[17] H.J. Kim, K.S. Kim, J.F. Wang, M. Sasaki, N. Satoh, et al., Dirac versus Weyl fermions in topological insulators: Adler-Bell-Jackiw anomaly in transport phenomena, Phys. Rev. Lett. 111 (24) (2013) 246603.
[18] X. Xu, W.H. Jiao, N. Zhou, Y. Guo, Y.K. Li, et al., Quasi-linear magnetoresistance and the violation of Kohler's rule in the quasi-one-

dimensional $Ta_4Pd_3Te_{16}$ superconductor, J. Phys. Condens. Matter 27 (33) (2015) 335701.
[19] Z.W. Zhu, J.H. Wang, H.K. Zuo, B. Fauqué, R.D. McDonald, et al., Emptying Dirac valleys in bismuth using high magnetic fields, Nat. Commun. (2017) 15297.
[20] C.L. Zhang, S.Y. Xu, C.M. Wang, Z. Lin, Z.Z. Du, et al., Magnetic-tunnelling-induced Weyl node annihilation in TaP, Nat. Phys. (2017), https://doi.org/10.1038/nphys4183.
[21] C. Shang, Z.C. Xia, M. Wei, Z. Jin, B.R. Chen, et al., Al^{3+} doping effects and high-field phase diagram of $La_{0.5}Sr_{0.5}Mn_{1-x}Al_xO_3$, J. Phys. D Appl. Phys. 49 (3) (2016) 035001.
[22] H.K. Zuo, L.R. Shi, Z.C. Xia, J.W. Huang, B.R. Chen, et al., The magnetic anisotropy and complete phase diagram of $CuFeO_2$ measured in a pulsed high magnetic field up to 75T, Chin. Phys. Lett. 32 (4) (2015) 047502.
[23] M.Y. Ruan, Z.W. Ouyang, S.S. Sheng, X.M. Shi, Y.M. Guo, et al., High-field magnetization study of spin-chain compounds $Ca_3Co_{2-x}Mn_xO_6$, J. Magnetism Magnetic Mater. 361 (2014) 157−160.
[24] B.R. Chen, Z.C. Xia, J.W. Huang, Z. Jin, H.K. Zuo, et al., Engineering of ion-doping on the ground states and Bose-Einstein condensation of $Sr_3Cr_2O_8$, Mater. Chem. Phys. 167 (2015) 278−285.
[25] C. Chen, Y.B. Han, X.J. Wang, P.P. Chen, J.B. Han, et al., Low temperature photo-induced carrier dynamics in the $GaAs_{0.985}N_{0.015}$ alloy, J. Alloys Compd. 699 (2017) 297−302.
[26] J. Zhang, X. Wang, Z. Zhong, Z. Ma, S. Wang, et al., Magnetic field induced extraordinary photoluminescence enhancement in Er^{3+}:YVO_4 single crystal, J. Appl. Phys. 118 (8) (2015) 083101.
[27] Y. Han, Z. Ma, J. Zhang, J. Wang, G. Du, et al., Hidden local symmetry of Eu^{3+} in xenotime-like crystals revealed by high magnetic fields, J. Appl. Phys. 117 (5) (2015) 055902.
[28] G. Du, P. Liu, W. Guo, Y. Han, J. Zhang, et al., The influence of high magnetic field on electric-dipole emission spectra of Eu^{3+} in different single crystals,, J. Mater. Chem. C 1 (45) (2013) 7608−7613.
[29] S.L. Wang, L. Li, Z.W. Ouyang, Z.C. Xia, N.M. Xia, et al., Development of high-magnetic-field, high-frequency electronic spin resonance system, Acta Phys. Sin. 61 (10) (2012) 107601.
[30] M.Y. Ruan, Z.W. Ouyang, Y.M. Guo, J.J. Cheng, Y.C. Sun, et al., Disappearance of Ising nature in Ca_3ZnMnO_6 studied by high-field ESR, J. Phys. Condens. Matter 26 (23) (2014) 236001.
[31] Y.F. Deng, T. Han, Z. Wang, Z. Ouyang, B. Yin, et al., Uniaxial magnetic anisotropy of square-planar chromium (II) complexes revealed by magnetic and HF-EPR studies, Chem. Commun. 51 (100) (2015) 17688−17691.
[32] V. Psyk, D. Risch, B.L. Kinsey, A.E. Tekkaya, M. Kleiner, Electromagnetic forming—a review, J. Mater. Process. Technol. 211 (5) (2011) 787−829.
[33] L. Li, X. Han, T. Peng, H. Ding, T. Ding, et al., Space-time-controlled multi-stage pulsed magnetic field forming and manufacturing technology, in: The 5th International Conference on High Speed Forming. Dortmund, Germany, 2012, pp. 53−58.
[34] Z. Lai, X. Han, Q. Cao, L. Qiu, Z. Zhou, et al., The electromagnetic flanging of a large-scale sheet workpiece, IEEE Trans. Appl. Supercond. 24 (3) (2014) 0500805.
[35] Q. Xiong, Q. Cao, X. Han, Z. Lai, F. Deng, et al., Axially movable electromagnetic forming system for large-scale metallic sheet, IEEE Trans. Appl. Supercond. 26 (4) (2016) 3701404.
[36] Z. Lai, Q. Cao, B. Zhang, X. Han, Z. Zhou, et al., Radial Lorentz force augmented deep drawing for large drawing ratio using a novel dual-coil electromagnetic forming system, J. Mater. Process. Technol. 222 (2015) 13−20.
[37] X. Zhang, Q. Cao, X. Han, Q. Chen, Z. Lai, et al., Application of triple-coil system for improving deformation depth of tube in electromagnetic forming, IEEE Trans. Appl. Supercond. 26 (4) (2016) 3701204.
[38] M.F. Hsieh, Y.M. Lien, D.G. Dorrell, Post-assembly magnetization of rare-earth fractional-slot surface permanent-magnet machines using a two-shot method, IEEE Trans. Industry Appl. 47 (6) (2011) 2478−2486.
[39] Y. Lv, G. Wang, L. Li, Post-assembly magnetization of a 100 kW high speed permanent magnet rotor, Rev. Sci. Instrum. 86 (3) (2015) 034706.
[40] Q. Cao, X. Han, L. Li, Configurations and control of magnetic fields for manipulating magnetic particles in microfluidic applications: magnet systems and manipulation mechanisms, Lab Chip 14 (15) (2014) 2762−2777.
[41] B. Polyak, G. Friedman, Magnetic targeting for site-specific drug delivery: applications and clinical potential, Expert Opin. Drug Deliv. 6 (1) (2009) 53−70.
[42] C. Plank, O. Zelphati, O. Mykhaylyk, Magnetically enhanced nucleic acid delivery, Ten years of magnetofection—progress and prospects, Adv. Drug Deliv. Rev. 63 (14) (2011) 1300−1331.
[43] L. Liang, C. Zhang, X. Xuan, Enhanced separation of magnetic and diamagnetic particles in a dilute ferrofluid, Appl. Phys. Lett. 102 (23) (2013) 234101.
[44] Q. Cao, X. Han, L. Chun, J. Liu, L. Li, Note: magnetic targeting for enhancement of the activation efficiency of G protein-coupled receptor with a two-pair coil system, Rev. Sci. Instrum. 87 (1) (2016) 016103.
[45] X. Han, Y. Feng, Q. Cao, L. Li, Three-dimensional analysis and enhancement of continuous magnetic separation of particles in microfluidics, Microfluidics Nanofluidics 18 (5−6) (2015) 1209−1220.
[46] Q. Cao, X. Han, L. Li, An active microfluidic mixer utilizing a hybrid gradient magnetic field, Int. J. Appl. Electromagn. Mech. 47 (3) (2015) 583−592.